Pressure and temperature-dependent Raman study of $YLiF_4$

E. Sarantopoulou, Y. S. Raptis, E. Zouboulis, and C. Raptis
Department of Physics, National Technical University, GR-15780, Athens, Greece
(Received 17 October 1997; revised manuscript received 26 October 1998)

Raman scattering spectra of single crystals of $YLiF_4$ have been measured over wide ranges of hydrostatic pressures (0–20 GPa) and temperatures (30–1000 K). Unlike other members of the scheelite crystal class, the internal modes of $YLiF_4$ due to vibrations within the LiF_4^{-3} tetrahedra display large $\partial\omega/\partial P$ and $\partial\omega/\partial T$ slopes. In contrast, all four external modes corresponding to lattice translations show small $\partial\omega/\partial T$ slopes, with one of them (whose observation from the pressure cell is clear) also showing a small $\partial\omega/\partial P$ slope. These results suggest that temperature or pressure affect primarily the dynamics of the LiF_4^{-3} group. This conclusion is further supported by an anharmonicity analysis in which the volume contribution to the total frequency shifts observed with temperature has been found very large for the internal modes. An abrupt change of slope in the frequency-versus-pressure diagrams of internal modes at 7 GPa is attributed to a stiffening of the LiF_4^{-3} group. From the anharmonicity analysis, it is concluded that the internal binding in the LiF_4^{-3} tetrahedra is essentially of ionic character. [S0163-1829(99)09805-7]

I. INTRODUCTION

$YLiF_4$ has been extensively used for several years as host material for various optically active rare-earth ions and the production of laser action.[1–5] Therefore, an understanding of the lattice dynamics of $YLiF_4$ is essential and, indeed, several relevant studies have been published[6–10] over the years reporting Raman[6–9] and IR[6–9] spectra as well as neutron diffraction[10] and molecular dynamics calculations.[10] The purpose of the present work is to extend such a lattice dynamics study under conditions of variable pressure and temperature.

At ambient conditions, $YLiF_4$ has the tetragonal scheelite ($CaWO_4$) structure (C_{4h}^6 space group) with two molecules in its unit cell[6,11] (Fig. 1). Most of the other alkaline earth tungstates and molybdates, such as $SrWO_4$,$BaWO_4$, $CaMoO_4$,$SrMoO_4$, etc., also crystallize in the scheelite structure. These salts consist of tightly bound XO_4^{-2} ($X=$W, Mo) tetrahedra which are linked to metal cations via weak ionic bonds. Because of the different force constants corresponding to the internally bound atoms in the tetrahedra on the one hand, and the lattice ions on the other, the vibrational frequencies of atoms within the XO_4^{-2} anions (''internal'' modes) are much higher than the frequencies of vibrations between lattice ions (''external'' modes).

In $YLiF_4$, the cation is Y^{+3} and the molecular anion LiF_4^{-3}. However, in contrast to the XO_4^{-2} anion of tungstates and molybdates, the internal binding in the LiF_4^{-3} tetrahedron is not as strong (it is considered[6] of about the same magnitude as the external lattice binding) which means there is no much difference between frequencies of ''internal'' and ''external'' modes. The internal/external division has been disputed for some modes of $YLiF_4$ in a recent molecular dynamics calculation[10] because of the strong mode coupling.

Group theoretical considerations predict the following irreducible representation for the zone center modes of the C_{4h}^6 (scheelite) space group:

$$3A_g+5B_g+5E_g+5A_u+3B_u+5E_u\,.$$

Of the Raman modes, 4 are external translational ($2B_g+2E_g$), 2 rotational (A_g+E_g) and 7 internal within the tetrahedron ($2A_g+3B_g+2E_g$).

In this article the Raman spectra of $YLiF_4$ are reported for wide ranges of hydrostatic pressures and temperatures, and $\partial\omega/\partial P$ and $\partial\omega/\partial T$ derivatives as well as Grüneisen parameters are obtained. Furthermore, the volume and pure temperature contributions to the total frequency shifts observed with temperature are evaluated for certain modes (whose symmetry identification and $\partial\omega/\partial P$ slopes are unambiguously determined), thus providing information about the type of bonds involved.

II. EXPERIMENTAL

A rectangular ($4\times4\times5$ mm^3) single crystal of $YLiF_4$ cut and polished along the crystallographic axes has been used for the temperature dependence measurements. Assuming a laboratory frame in which the axes *x,y,z*, coincide with the crystallographic axes *a,b,c*, respectively, the following 90° scattering configurations have been used: $y(zz)x$ giving A_g symmetry phonons, $y(xy)x$ giving B_g phonons, and $y(zy)x$ in which E_g phonons are observed.

For the high pressure experiments, small single crystal

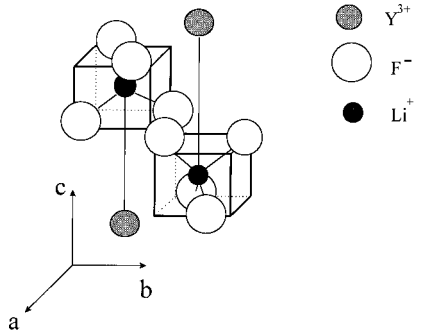

FIG. 1. Unit cell of $YLiF_4$.

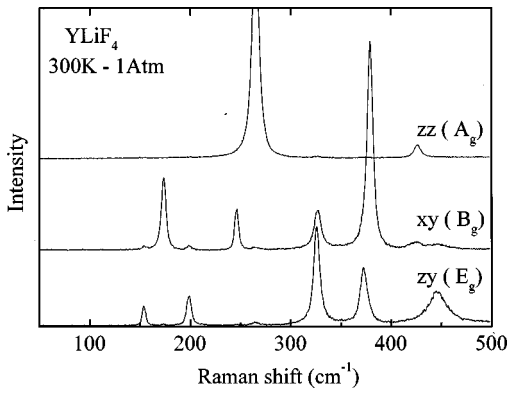

FIG. 2. Polarized $y(zz)x$, $y(xy)x$, and $y(zy)x$ Raman spectra of $YLiF_4$ at ambient conditions corresponding to the A_g, B_g, and E_g phonon symmetries.

samples (typical dimension $\approx 50\ \mu$m) have been inserted in a Diamond Anvil Cell (DAC) together with ruby chips for monitoring the pressure. A solution of methanol-ethanol has been used as pressure transmitting medium which displays hydrostatic behavior up to 11 GPa and only small deviations (up to 2.5%) from this behavior for the range 11–20 GPa.

The low temperature measurements have been performed inside a closed cycle He cryostat. For the high temperature experiments, the sample was held inside a silica cell in Ar atmosphere which was centrally positioned inside a vacuum operated optical furnace of low temperature gradients.

The 496.5 nm Ar^+ laser line has been used for the excitation of Raman spectra since it does not excite any luminescence emission in the spectral region close to the line. Spectral analysis and detection of scattered light have been accomplished by a double monochromator in line with a cooled photomultiplier and photon counting equipment. The spectral resolution has been 2.5 cm^{-1} for the temperature dependent measurements and 3.5 cm^{-1} for the pressure ones.

III. RESULTS

Figure 2 shows the *zz*, *xy* and *zy* components of the Raman spectrum of $YLiF_4$ at ambient conditions giving the A_g, B_g and E_g symmetry phonons respectively. Some of the observed weak features result from polarizer leakages of strong lines belonging to different phonon symmetries. The frequencies of all Raman phonons of $YLiF_4$ at room temperature measured in this work and in previous studies are listed in Table I. One A_g phonon had escaped detection until recently when Salaun *et al.*[9] reported it at 151 cm^{-1}. We have also observed this extremely weak peak, which is just above noise level [Fig. 3(a)], by careful polarization measurements around this spectral region using slower scans. To make sure that this peak is not a polarization leak of the nearby E_g mode at 154 cm^{-1}, we recorded at identical conditions the *yz* component [Fig. 3(b)] and found no such interference on the *zz* component by the E_g mode. Instead, some of the spectral activity at 175 cm^{-1} in the *zz* spectrum [Fig. 3(a)] is most likely due to a polarization leak of the strong B_g phonon of the *xy* spectrum.

Raman spectra of $YLiF_4$ at various pressures are shown in Fig. 4, while Fig. 5 illustrates the pressure dependence of the phonon frequencies. An apparent decrease of slope is observed around 7 GPa in almost all plots of Fig. 5. We have confirmed that this change of slope is discontinuous by performing a series of data point fittings for the phonons at 326 and 446 cm^{-1} which show the largest slopes and slope changes. First, we fitted the data points of each phonon to a quadratic function and then we performed a sequence of two linear fittings for each phonon, each time assuming a different value of critical pressure (assumed data point in which the slope changes) on both sides of the 7 GPa value. The standard deviation (chi-squared) of the two fitting procedures have been plotted against the assumed critical pressure for

TABLE I. Frequencies (in cm^{-1}) and assignment of Raman active phonons of $YLiF_4$ (300 K, 1 atm).

Ref. 6	Ref. 7	Ref. 8	Ref. 9	This work	Phonon symmetry
			151	151	A_g
153	158	149	154	154	E_g
177	177	167	174	173	B_g
199	203	193	199	198.5	E_g
248	251	241	246	246	B_g
264	269	261	265	265	A_g
329	329	322	326	326	E_g
329	331	323	327	326.5	B_g
368	376	369	373	372.5	E_g
382	382	375	379	379	B_g
425	426	422	427	426	A_g
427	430	423	427	426	B_g
446	450	442	447	446	E_g

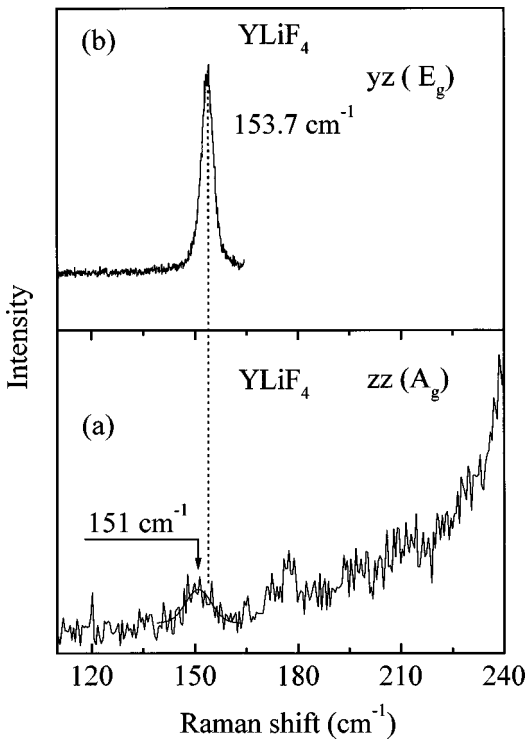

FIG. 3. Polarized *zz* Raman spectrum (a) of $YLiF_4$ at ambient conditions in the low frequency region showing the very weak A_g phonon at 151 cm^{-1}; to make sure this is not a polarization leak, the *yz* spectrum is also given (b) showing the nearby E_g phonon at 154 cm^{-1}.

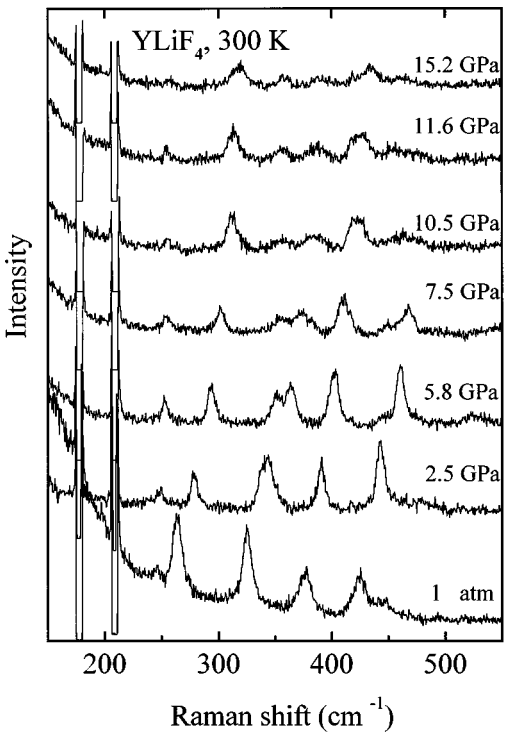

FIG. 4. Raman spectra of $YLiF_4$ for various hydrostatic pressures (0–15.2 GPa).

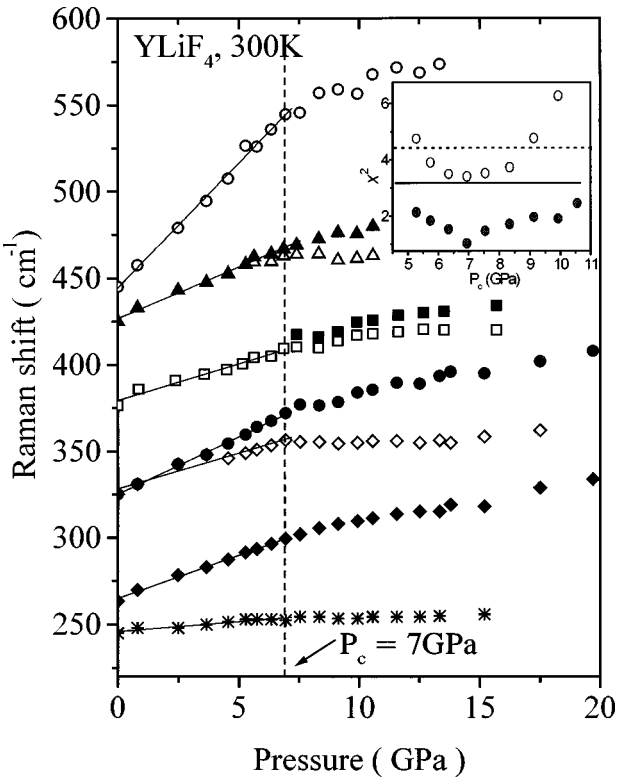

FIG. 5. Pressure dependence of phonon frequencies of the Raman active modes of $YLiF_4$. The solid lines are linear least-squares fittings giving the $\partial\omega/\partial P$ slopes. The error bars are up to ± 1.5 cm^{-1} and ± 0.05 GPa in the vertical and horizontal axes respectively for $P \leqslant 10.5$ GPa, and ± 2–5 cm^{-1} and ± 0.1–0.4 GPa for $P > 10.5$ GPa (they increase with increasing pressure). Inset: standard deviations (chi squares) of quadratic (straight lines) and two-line linear fittings (circles) for the pressure data points, plotted against pressure, for the phonons at 326 (full circles and solid line) and 446 cm^{-1} (open circles and dotted line); see text for details.

the two phonons and are shown in the inset of Fig. 5. In both cases, the data points fit better to two linear functions and this confirms that the change of slope is discontinuous. Furthermore, this series of fittings confirm also that the slope changes at 7 GPa. Possible causes for these changes are discussed in the following section. From the low pressure linear fitting, the $\partial\omega/\partial P$ slopes and Grüneisen parameters $\gamma = \partial \ln \omega / \partial \ln V$ have been deduced and are given in Table II. (see Sec. IV E for details concerning the volume compressibility used for the calculation of the Grüneisen parameters).

The low frequency E_g phonons at 154 and 198.5 cm^{-1} are just about observed inside the DAC as their intensity is at the noise level, which makes the determination of their frequency shifts with pressure difficult. Because of this, we have not included their plots and $\partial\omega/\partial P$ slopes in Fig. 5 and Table II, respectively. Detection of the B_g phonon at 173 cm^{-1} inside the DAC is obscured by the presence of a plasma line whose position coincides with the frequency of the phonon; however, since this phonon does not emerge at high pressures, it is concluded that it is either pressure independent or its $\partial\omega/\partial P$ is very small. All clearly observed phonons display normal mode behavior, that is, they harden with increasing pressure. The slope $\partial\omega/\partial P$ of the phonons appears, on the whole, to increase with increasing phonon frequency.

Six peaks are clearly observed at ambient pressure inside the DAC, three of which are doublets (326–326.5 cm^{-1}, 372.5–379 cm^{-1}, and 426–426 cm^{-1}), corresponding to two phonons of different symmetries (see also Table I). The doublet at 326 cm^{-1} splits at about 4 GPa as a consequence of the different $\partial\omega/\partial P$ slopes of the two (B_g and E_g) phonons. Given that polarized Raman measurements are quite difficult to obtain inside the DAC, unambiguous assignment of the two resolved peaks is not possible. A one line fitting has been used for the doublet around 375 cm^{-1} below P_c (Fig. 5) as the two components do not appear to separate, thus obtaining the same $d\omega/dP$ slopes for the two phonons (Fig. 5 and Table II). Above P_c, this doublet initially broadens and above 10 GPa displays a flat (square-like) shape, most likely

TABLE II. Frequencies of phonons of $YLiF_4$ observed at ambient conditions inside the pressure cell, along with their pressure derivatives and mode Grüneisen parameters at 300 K. The Grüneisen parameters were determined using a value $k = 1.24 \times 10^{-2}$ GPa^{-1} which was calculated from the experimental elastic constant data of Ref. 27 according to Eqs. (11) and (12).

Phonon frequency (cm^{-1})	$d\omega/dp$ (cm^{-1}/GPa)	γ^T
246(B_g)	1.13	0.368
265(A_g)	5.00	1.501
326(E_g+B_g)	4.13	0.963
	6.66	1.66
375(E_g+B_g)	4.54	0.973
426(A_g+B_g)	5.77	0.956
446(E_g)	14.43	2.519

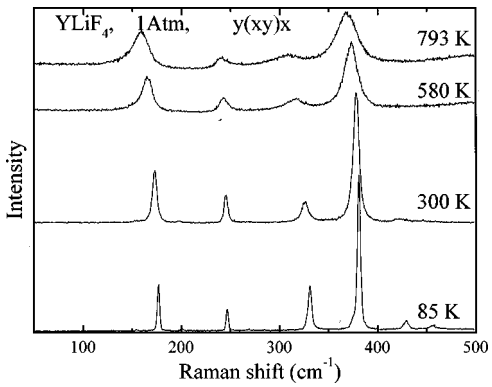

FIG. 6. Polarized $y(xy)x$ Raman spectrum of $YLiF_4$ at various temperatures (85–793 K).

because of a gradual mode separation; for this reason, we have performed a two line fitting for this doublet above P_c, which shows a gradual separation of the two peaks. However, unambiguous assignment of the two modes is not also possible for this doublet. Finally, the doublet at 426 cm^{-1} starts resolving at $\approx$6 GPa, showing a continuous increase of spectral distance between the two modes. The remaining three peaks observed from the DAC are unambiguously identified as the B_g, A_g and E_g modes at 246, 265 and 446 cm^{-1}, respectively.

The $y(xy)x$ component of the Raman spectrum of $YLiF_4$ is shown in Fig. 6 for various temperatures, while the temperature dependence of frequencies of 12 phonons are given in Fig. 7. (It is difficult to determine the temperature dependence of the very weak A_g phonon at 151 cm^{-1}.) The experimental points of Fig. 7 are fitted by the following polynomial function:

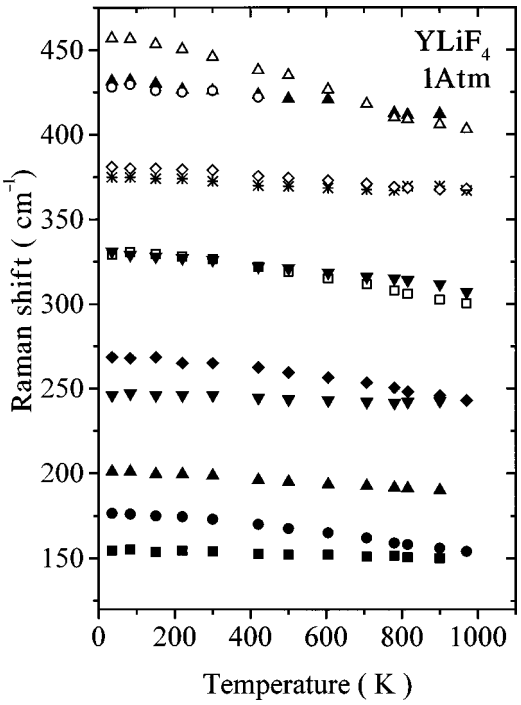

FIG. 7. Temperature dependence of phonon frequencies of the Raman active modes of $YLiF_4$. The error bars are ± 0.5 cm^{-1} and ± 1 K in the vertical and horizontal axes respectively for $T \leqslant 300$ K, and up to ± 1 cm^{-1} and ± 3 K for $T > 300$ K.

TABLE III. Mode frequencies of $YLiF_4$ at 0 K obtained by extrapolation of the fitting to the function of Eq. (1), their temperature derivatives at 300 K, and fitting values of the parameters in Eq. (1).

ω_0 (cm^{-1})	$(d\omega/dT)_{300\,K}$ (cm^{-1}/K)	a_1 (10^{-3} cm^{-1}/K)	a_2 (10^{-5} cm^{-1}/K^2)
154.9(E_g)	−0.005	−4.6	−0.08
177.4(B_g)	−0.020	−13.3	−1.19
201.8(E_g)	−0.013	−13.1	−0.02
246.7(B_g)	−0.006	−2.5	−0.57
269.2(A_g)	−0.021	−9.8	−2.00
331.4(B_g)	−0.026	−14.2	−2.00
330.7(E_g)	−0.020	−15.0	−0.80
376.0(E_g)	−0.012	−13.5	−0.22
381.9(B_g)	−0.015	−13.6	−0.23
432.8(A_g)	−0.023	−21.1	−0.40
428.9(B_g)	−0.018	−11.0	−1.10
460(E_g)	−0.057	−48.0	−2.00

$$\omega(T) = \omega_0 + \alpha_1 T + \alpha_2 T^2. \quad (1)$$

The fitting values $\omega_0, \alpha_1, \alpha_2$, together with the slopes $\partial\omega/\partial T$ for 12 phonons at 300 K, are given in Table III. All phonons display normal temperature dependence, that is, negative $\partial\omega/\partial T$ slopes.

IV. DISCUSSION

A. Raman spectra of $YLiF_4$ at ambient conditions

Our assignment of phonon symmetries for $YLiF_4$ (Table I) is based on polarized Raman measurements and is in agreement with previous reports.[6–9] The phonon frequencies of this work are in very good agreement with those of Ref. 9, but less so with other previous works.[6–8]

The atomic motions corresponding to the 13 Raman symmetry species of $YLiF_4$ were reported by Miller *et al.*[6] Recently, Salaün *et al.*[10] performed a molecular dynamics calculation in $YLiF_4$ using a rigid ion model and reported that certain Raman (and IR) modes cannot be assigned to simple atomic motions proposed by Miller *et al.*[6] (but to a combination of such motions) because of strong mode couplings. Although, couplings between internal and external modes are anticipated in a crystal with not so strong internal binding, it is difficult to realize that such interactions alter drastically the character of the modes, in view also of the experimental evidence that the low frequency modes ($2B_g + 2E_g$) are very sensitive to rare-earth substitution[7–10] for Y, while the high frequency B_g and E_g modes and all the A_g modes are either moderately or not sensitive at all.[7,8]

Because of this strong experimental evidence, we shall retain the internal/external characterization for all modes in $YLiF_4$. In this situation, the $2B_g$ and $2E_g$ phonons at low frequencies (Table I), being sensitive to rare-earth substitution, correspond to external (lattice) modes, i.e., motions of Y^{3+} or translations of whole formula units according to Ref. 6. The two rotational modes should be the A_g at 151 cm^{-1} and the E_g at 326 cm^{-1} because they are barely sensitive to rare-earth substitution; the rotational character of this A_g

mode is further supported by the fact that it is the weakest among all A_g modes. The remaining high frequency modes should be due mainly to motions within the LiF_4^{-3} tetrahedron.

B. Pressure dependence of Raman phonons

Of the 4 external modes, only the phonon at 246 cm^{-1} is observed clearly in the DAC, showing a small $\partial\omega/\partial P$ slope (Fig. 5, Table II). In contrast, the internal modes and the rotational E_g mode at 326 cm^{-1} appear to be strongly pressure dependent, thus confirming the idea[6] that the binding within the LiF_4^{-3} anion is not as strong as in tungstates and molybdates. Jayaraman *et al.*[12,13] observed abrupt decreases of phonon frequencies with pressure in $BaWO_4$ (Ref. 12), and in $PbMoO_4$ and $PbWO_4$ (Ref. 13) and attributed these effects to a first order phase transition to monoclinic wolframite (C_{2h}^4) or monoclinic $HgMoO_4$ (C_{2h}^6) structure. Similar frequency discontinuities have been observed by Christofilos *et al.*[14] for $CaMoO_4$ at 8.2 and 15 GPa who concluded the occurrence of two phase transitions for this crystal, with the first at 8.2 GPa to one of the monoclinic structures mentioned above.

In the case of $YLiF_4$, all internal modes sustain abrupt decreases of slope at $P_c = 7$ GPa (Fig. 5), but there are no frequency discontinuities or new Raman bands observed above this pressure. Therefore, the possibility of a structural phase transition is remote but it should not be excluded altogether because Raman signals from the DAC at high pressures are low and some weak peaks may not be detectable. Most likely, this slope decrease is due to a stiffening of the tetrahedral LiF_4^{-3} group (it becomes less compressible) because of force constant changes, but without any change of its coordination. It appears that $YLiF_4$ remains tetragonal C_{4h}^6 above P_c, with the only structural change justified by these slope decreases being a possible change of the Li-F distances rather than the Y^{+3}-LiF_4^{-3} ones.

C. Temperature dependence of Raman phonons in $YLiF_4$

The Raman phonons of $YLiF_4$ show normal mode behavior with temperature, that is, negative $\partial\omega/\partial T$ slopes in their frequency plots (Fig. 7), without any sign of instability or discontinuity. Hence, $YLiF_4$ remains stable over the range 30–1000 K.

In a molecular crystal, it is expected that the internal modes should display small $\partial\omega/\partial P$ and $\partial\omega/\partial T$ because of the strong internal binding of the molecular groups involved. This is not the case with $YLiF_4$ for which very large slopes are obtained for some internal modes (Table II). Hence, $YLiF_4$ does not behave like a typical molecular crystal.

D. Anharmonicity analysis

In temperature-dependent Raman measurements, there are two contributions to the observed phonon frequency shifts;[15–23] (i) one results from thermal expansion which alters the interatomic distances and consequently the binding forces (volume or implicit effect) and (ii) the other is due to pure temperature effect and it is associated with anharmonic phonon interaction and decay (anharmonic or explicit effect). If one combines temperature and pressure Raman results, the two contributions can be separated and estimated using the following expression:

$$\left(\frac{\partial\omega}{\partial T}\right)_P = -\frac{\beta}{\kappa}\left(\frac{\partial\omega}{\partial P}\right)_T + \left(\frac{\partial\omega}{\partial T}\right)_V, \tag{2}$$

where $(\partial\omega/\partial T)_P$ is the (isobaric) variation of ω with temperature as measured in temperature Raman experiments (total effect), $(\partial\omega/\partial P)_T$ is the (isothermal) change of ω with pressure as measured in pressure Raman experiments (volume contraction), $\beta(T)$ is the volume thermal expansion coefficient and $\kappa(T)$ is the volume compressibility. The first term on the right of Eq. (2) represents the volume effect, while the term $(\partial\omega/\partial T)_v$ is the (isochoric) variation of ω with T (anharmonic effect), a quantity which cannot be measured but can be calculated from Eq. (2).

The ratio of the volume term to the total variation (Eq. 2)

$$\eta = -\frac{\beta}{\kappa}\frac{(\partial\omega/\partial P)_T}{(\partial\omega/\partial T)_P} \tag{3}$$

is a dimensionless parameter introduced by Weinstein and Zallen[17] in order to determine the relative importance of the two effects. This parameter, known as the implicit fraction, may assume values between 0 and ∞ and largely indicates the type of crystal bonding associated with the particular mode. For η approaching zero, the explicit effect is almost entirely responsible for the frequency shift observed in Raman measurements under variable temperature, implying that the crystal bonding is essentially covalent or, in the case of molecular crystals, the internal binding of molecular groups is strong;[17] in either case, thermal expansion does not affect the forces involved. For $\eta = 1$, thermal expansion is exclusively responsible for the observed frequency shifts, indicating that the crystal bonding is of ionic character. For $\eta = 0.5$ ($\eta = \infty$), the contributions of the two effects to the total observed shift are comparable and have the same (opposite) sign. When the volume effect is dominant with a small explicit contribution of the opposite sign, the parameter η takes finite values above unity.

The integrated form of Eq. (2) is

$$\Delta\omega_{\mathrm{tot}}(T) = \Delta\omega_{\mathrm{vol}}(T) + \Delta\omega_{\mathrm{expl}}(T) \tag{4a}$$

or

$$\Delta\omega_{\mathrm{expl}}(T) = \Delta\omega_{\mathrm{tot}}(T) - \Delta\omega_{\mathrm{vol}}(T), \tag{4b}$$

which makes possible the separation of the two effects in terms of frequency shifts instead of their derivatives. The total frequency shifts $\Delta\omega_{\mathrm{tot}}(T)$ are obtained from Fig. 7 or Eq. (1) and the volume driven shift from

$$\Delta\omega_{\mathrm{vol}}(T) = -\int_0^T \frac{\beta(T')}{\kappa(T')}\left(\frac{\partial\omega}{\partial P}\right)_{T'} dT'. \tag{5}$$

It has been found in other materials[20,21] that $(\partial\omega/\partial P)_T$ slopes vary little with temperature and, therefore, they can be considered constant in the integral of Eq. (5).

Strictly speaking, the above analysis and Eq. (2) are valid only for isotropic crystals of cubic symmetry for which the phonon frequency is a function of two variables: volume

and temperature, $\omega=\omega(V,T)$. For a uniaxial crystal, though, such as $YLiF_4$, the phonon frequency is a function of three variables, namely the crystal lattice parameters a and c (the c/a ratio is not constant with temperature), and temperature: $\omega=\omega(a,c,T)$. Certain corrections to isotropic approximation were introduced by Peercy[15] in the case of tetragonal TiO_2 by considering uniaxial stress Raman data and repeated later by Cerdeira *et al.*[19] and Liarokapis *et al.*[20] in other uniaxial crystals. In a recent work,[23] a complete analysis has been carried out in order to derive the correct expression of Eq. (2) for a uniaxial crystal and calculate the percentage deviation of the isotropic approximation from the accurate uniaxial approach. For such an accurate analysis, it is necessary to have uniaxial stress Raman data available, but in the absence of such data for $YLiF_4$, all calculations will be performed using the isotropic approximation.

The low signal to noise ratio of the four lowest frequency modes and the difficulty in identifying the phonon symmetries of the components of the doublets in the DAC Raman experiments, restricts the anharmonicity analysis to only five modes. Three of them are unambiguously assigned in these experiments, namely the external B_g mode at 246 cm^{-1}, and the internal A_g and E_g modes at 265 and 446 cm^{-1}, respectively. We have also carried out an anharmonicity analysis for the doublet at about 375 cm^{-1} $[372.5(E_g)-379(B_g)]$. As was mentioned, the components of this doublet cannot be identified in the pressure dependent measurements below 7 GPa and for this reason a common $d\omega/dP$ slope has been determined for the two components by a one line fitting (Fig. 5 and Table II). In the temperature dependent measurements, though, the two components of this doublet are clearly identified and their $d\omega/dT$ slopes definitely determined (-0.012 and -0.015 cm^{-1}/K for the E_g and B_g phonons respectively). Thus, using the common $d\omega/dP$ slope and the above mentioned $d\omega/dT$ slopes, we can perform an anharmonicity calculation for these phonons.

E. Thermal expansion coefficient and compressibility of $YLiF_4$

In anharmonicity studies, it is often frustrating when one reaches the stage of analysis which involves the introduction to calculations of the thermal expansion coefficient and compressibility of the material. There are only a few materials for which these parameters have been measured over extended temperature ranges. In the case of $YLiF_4$, the temperature dependence of the lattice parameters has been measured by Blanchfield *et al.*[24] in the range 170–825 K and by Misiak *et al.*[25] for four temperatures, namely 93, 153, 213, and 293 K. We have used average values of lattice parameters in the region of temperature overlap of these studies[24,25] and then we calculated the volume expansion coefficient in the range 93–825 K from the expression:

$$\beta(T)=\frac{2}{a(T)}\frac{\Delta a(T)}{\Delta T}+\frac{1}{c(T)}\frac{\Delta c(T)}{\Delta T}. \tag{6}$$

For $T<93$ K there are no data concerning thermal expansion and because of this we have used approximate values of $\beta(T)$ as calculated from the Debye temperature data of Gluyas *et al.*[26] for the isomorphous $CaWO_4$ using the formula[22]

$$\beta(T)=\beta_\infty D(\xi)=\beta_\infty D(\Theta_D/T), \tag{7}$$

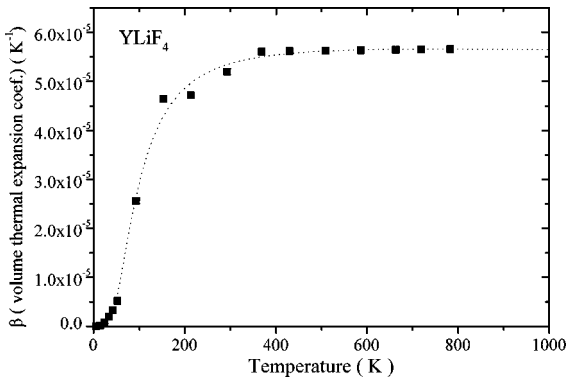

FIG. 8. Volume thermal expansion coefficient β for $YLiF_4$ in the range 0–790 K (see text for details).

where

$$D(\xi)=\frac{3}{\xi^3}\int_0^{\xi}\frac{x^4}{(e^x-1)^2}dx \tag{8}$$

is the Debye integral and $\beta_\infty=\beta(300)/D(\Theta_D/300)$ is the high temperature limiting value of $\beta(T)$. It should be pointed out that according to Gluyas *et al.*[26] $\Theta_D=246$ K at $T\approx 0$ K for $CaWO_4$. We note here that there are additional and rather controversial data in the literature[27] for the low temperature limiting value of the Θ_D for $CaWO_4$ varying between 230 and 285 K. In the case of $YLiF_4$, the only value existing from independent measurements is the low temperature limiting value $\Theta_D=279$ K at $T=4.3$ K (Ref. 27) which falls within the above mentioned range of values for $CaWO_4$. Therefore, in the absence of temperature dependence Θ_D data on $YLiF_4$, it is reasonable to use the data of the isomorphous $CaWO_4$ for $T<93$ K. Combining the experimental values for $\beta(T)$ as obtained from Eq. (6) and the estimated values[26] for $\beta(T)$ from Eqs. (7) and (8), we have fitted all these data points to the function[20–23]

$$\beta(T)=(A/T+B/T^2)\sinh^{-2}(T_1/T) \tag{9}$$

and the rather satisfactory fitting is shown in Fig. 8. The fitting parameters A, B and T_1 are given in Table IV. Values of $\beta(T)$ for $T>823$ K have been obtained by extrapolating the function of Eq. (9).

Using the fitted data of Fig. 8 and having in mind the definition of $\beta(T)$, we calculate the volume expansion from equation:

$$\left(\frac{\Delta V}{V}\right)_P=\int_{T_1}^{T_2}\beta(T)dT. \tag{10}$$

We find $(\Delta V/V)_P=10\%$ for the range 4–1000 K.

TABLE IV. Fitting values of the parameters in Eqs. (9) and (12).

$\beta(T)$	$A=-4\times10^{-5}$	$B=1.3$ (K)
	$T_1=149$ (K)	
$\kappa(T)$	$C=10.63\times10^{-3}$ (GPa^{-1})	$D=3.87\times10^{-6}$ ($GPa^{-1}K^{-1}$)
	$E=328.2$ (K)	

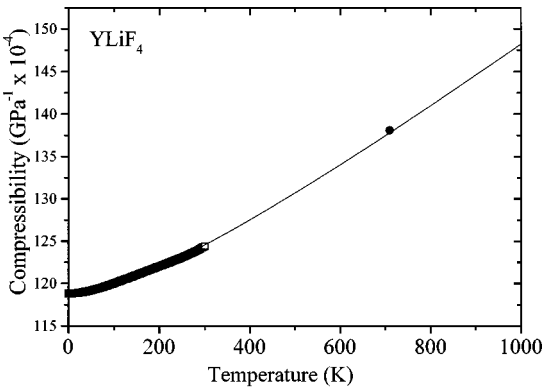

FIG. 9. Volume compressibility κ for $YLiF_4$; the data in the range 4.2–300 K are based on experimental measurements (see text for the extra point at 700 K).

The temperature dependence of the elastic constants c_{ij} of $YLiF_4$ has been measured by Blanchfield and Saunders[27] in the range 4.2–293 K from which the volume compressibility can be calculated

$$\kappa = \frac{c_{11}+c_{12}+2c_{33}-4c_{13}}{(c_{11}+c_{12})c_{33}-2c_{13}^2}. \tag{11}$$

The values of κ obtained in this way have been fitted to the expression[20–22]

$$\kappa(T) = C + DT + \frac{DE^2}{T+E}. \tag{12}$$

For $T>300$ K, values of κ were obtained by extrapolating the fitting of the experimental points of the 4.2–300 K range, assuming a linear dependence of κ at high temperatures (as is the case in other dielectric crystals[20–23]) and an estimated value of $1.38\times10^{-2}\,\mathrm{GPa}^{-1}$ at 700 K based on a slope equal to that of the isomorphous $CaMoO_4$.[28] The results of this fitting are shown in Fig. 9, while the fitting constants *C*, *D* and *E* are given in Table IV.

F. Contributions of volume and explicit effects to the total frequency shifts observed in $YLiF_4$ under variable temperature

Equations (2) and (4) have been used to separate the contributions of the volume and explicit effects and Eq. (5) to calculate the volume induced shift $\Delta\omega_{\mathrm{vol}}$. As was mentioned in Sec. IV D of this chapter, this analysis has been carried out for 5 out of the 13 Raman phonons.

The contributions $\Delta\omega_{\mathrm{vol}}$ and $\Delta\omega_{\mathrm{expl}}$ to the total shift for 5 phonons of $YLiF_4$ are shown in Fig. 10 plotted against temperature, while plots of the implicit fraction η for these phonons are shown in Fig. 11. The error bars for $\Delta\omega_{\mathrm{vol}}$ and $\Delta\omega_{\mathrm{expl}}$ were estimated at various temperatures above 200 K from Eqs. (5) and (4b) respectively by propagating the errors of directly and indirectly measured quantities. Below 200 K, all $\Delta\omega$'s (including the total shift) are very small, so that it serves no purpose to estimate their errors which are comparable in magnitude. In addition, for $T>200$ K the thermal expansion coefficient (obtained from experimental data) is practically constant, thus making the estimation of errors convenient. Error bars of up to $\pm8\%$ were estimated for both

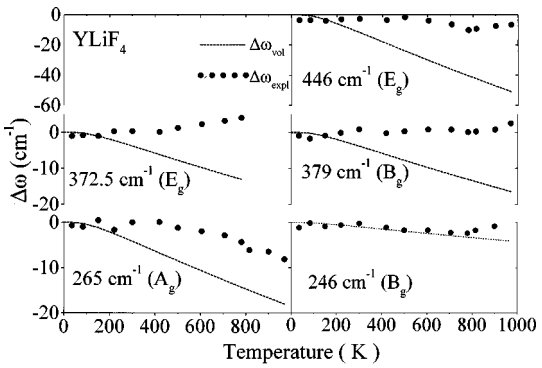

FIG. 10. Thermal expansion (dashed lines) and anharmonic (full circles) contributions, to the total frequency shifts of $YLiF_4$ as functions of temperature. The error bars for both $\Delta\omega_{\mathrm{vol}}$ and $\Delta\omega_{\mathrm{expl}}$ are up to $\pm8\%$ for $T>200$ K. Estimation of the error bars for $T<200$ K is meaningless because all $\Delta\omega$'s (including the total shift) are very small (see text for details).

$\Delta\omega_{\mathrm{vol}}$ and $\Delta\omega_{\mathrm{expl}}$ over various temperatures and modes. Similar procedure was followed for the estimation of the error bars for the implicit fraction η, i.e., by using Eq. (3) and propagating the errors of the quantities involved; these error bars were found about $\pm15\%$.

In the external mode at 246 cm^{-1} (translation of Y^{3+} along the *c*-axis), the thermal expansion and anharmonicity induced shifts are small, comparable and of the same sign

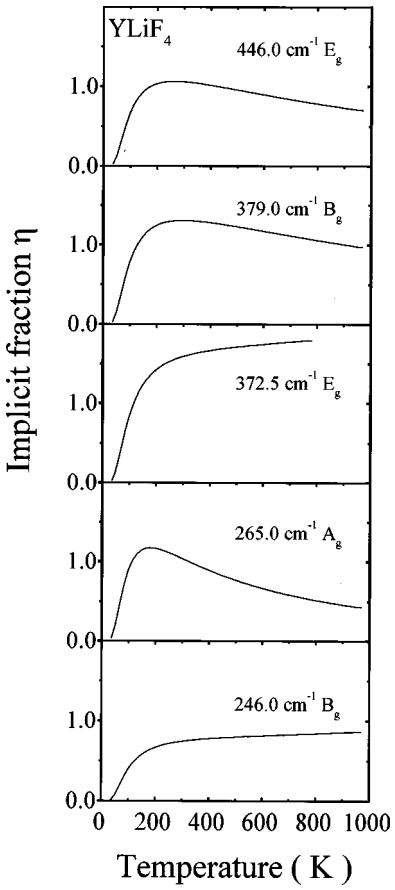

FIG. 11. Implicit fraction η for 5 phonons of $YLiF_4$ plotted against temperature. Typical error bars for η are about $\pm15\%$ for $T>200$ K (see text for details).

(downward shifts Fig. 10). The implicit fraction η for this phonon has an average value of ~ 0.7 and never exceeds the value of 0.8, thus indicating that the character of the external binding is not entirely ionic. Unfortunately, due to poor signal to noise ratio in the pressure experiments, we cannot generalize this conclusion for all external modes.

The four internal modes for which an anharmonicity analysis is possible, display frequency shifts with temperature which are almost entirely due to large downward $\Delta\omega_{\mathrm{vol}}$ shifts (Fig. 10). The anharmonicity contribution is small and of the same sign for the A_g and E_g modes at 265 and 446 cm^{-1}, but of opposite sign for the E_g and B_g phonons at 372.5 and 379 cm^{-1}. These observations essentially imply an ionic Li-F bonding in the LiF_4^{-3} group. Similar conclusions can be drawn upon examining the graphs of implicit fraction η for the internal modes (Fig. 11), which show values $\eta \cong 1$ for $T > 150\,\mathrm{K}$.

At low temperatures η tends to zero for any crystal[19–23] (because the thermal expansion coefficient tends to zero; see Fig. 8), thus incorrectly implying a drastic change in the nature of the bonding. Therefore, consideration of the implicit fraction η for determining the contribution of the two effects and the nature of the bonding is appropriate only above certain temperature at which the thermal expansion coefficient assumes a reasonable value. In general, bearing in mind the large margins of error involved at low temperatures, such anharmonicity studies are meaningful above certain temperature, which for $YLiF_4$ is about 200 K.

The anharmonicity study of both external and internal modes of $YLiF_4$ has provided evidence that temperature affects more, through thermal expansion, the dynamics of the LiF_4^{-3} group than the lattice dynamics. These results imply weak intramolecular forces and rather strong intermolecular ones and suggest that any structural change in the crystal is more likely to occur through a modification of the LiF_4^{-3} coordination.

V. CONCLUSIONS

The pressure and temperature dependence of the Raman active phonons of $YLiF_4$ have confirmed that this material does not behave like a typical molecular crystal and this conclusion is further supported by the anharmonicity analysis carried out. In contrast to isomorphous tungstates and molybdates, the internal modes of $YLiF_4$ due to intramolecular vibrations of the tetrahedral LiF_4^{-3} groups show large $\partial\omega/\partial P$ and $\partial\omega/\partial T$ slopes. This result, together with the fact that the volume contribution to the total frequency shifts observed with temperature dominates over anharmonicity in the case of the internal modes, suggest that temperature does not affect significantly the lattice dynamics of the crystal, but it does affect the internal dynamics of the LiF_4^{-3} group. Also judging from the pressure dependence of the 246 cm^{-1} external mode and, to certain extent, the presumably small $\partial\omega/\partial P$ slope of the 173 cm^{-1} external mode (which is obscured by a plasma line throughout the pressure range), we suggest with caution that pressure also should not affect the lattice dynamics to the degree it affects the internal dynamics. Hence, the conclusions of this work are in agreement with the accepted view for the existence of a strong crystal field[1,8,29] in this material, a property which justifies its use as host for laser activated ions.

Furthermore, the results of this work suggest that any structural modification in this crystal should be primarily mediated through a change of coordination of the LiF_4^{-3} group. The material is stable over the entire temperature range (30–1000 K) of its study. The change of slope in the phonon frequency plots at 7 GPa most likely indicates a stiffening of the LiF_4^{-3} group at this pressure. Finally, from the anharmonicity analysis it is concluded that the bonding in the LiF_4^{-3} group is essentially of ionic character.

ACKNOWLEDGMENTS

We are grateful to the General Secretariat for Research and Technology of Greece for partial support of this work. We should like to thank Professor W. Hayes and D. Manning of Clarendon Laboratory, University of Oxford for providing an oriented single crystal of $YLiF_4$.

[1] A. A. Kaminskii, *Laser Crystals*, 2nd ed. (Springer, Berlin, 1990), and references therein.

[2] A. L. Harper, A. Linz, and D. R. Gabbe, J. Phys. Chem. Solids **30**, 1483 (1969).

[3] J. E. Murray, IEEE J. Quantum Electron. **QE-19**, 488 (1983).

[4] T. M. Pollak, W. F. Wing, R. J. Grasso, E. P. Chicklis, and H. P. Jenssen, IEEE J. Quantum Electron. **QE-18**, 159 (1982).

[5] Z. Kollia, E. Sarantopoulou, A. C. Cefalas, M. A. Dubinskii, C. A. Nicolaides, R. Yu. Abdulsabirov, S. L. Korableva, A. K. Naumov, and V. V. Shemashko, J. Opt. Soc. Am. B **12**, 782 (1995).

[6] S. A. Miller, H. E. Rast, and H. H. Caspers, J. Chem. Phys. **52**, 4172 (1970).

[7] E. Schulteiss, A. Scarman, and D. Schwabe, Phys. Status Solidi B **138**, 465 (1986).

[8] X. X. Zhang, A. Schulte, and B. H. T. Chai, Solid State Commun. **89**, 181 (1994).

[9] S. Salaün, M. T. Fornoni, A. Bulou, M. Rousseau, P. Simon, and J. Y. Gesland J. Phys.: Condens. Matter **9**, 6941 (1997).

[10] S. Salaün, A. Bulou, M. Rousseau, B. Hennion, and J. Y. Gesland J. Phys.: Condens. Matter **9**, 6957 (1997).

[11] R. W. G. Wyckoff, *Crystal Structures*, 2nd ed. (Interscience Publishers, New York, 1964), Vol. 3, p. 19.

[12] A. Jayaraman, B. Batlogg, and L. G. VanUitert, Phys. Rev. B **28**, 4774 (1983).

[13] A. Jayaraman, B. Batlogg, and L. G. VanUitert, Phys. Rev. B **31**, 5423 (1985).

[14] D. Christofilos, G. A. Kourouklis, and S. Ves, J. Phys. Chem. Solids **56**, 1125 (1995).

[15] P. S. Peercy, Phys. Rev. B **8**, 6018 (1973).

[16] R. Zallen and M. L. Slade, Phys. Rev. B **18**, 5775 (1978).
[17] B. A. Weinstein and R. Zallen, in *Topics in Applied Physics*, edited by M. Cardona and G. Guntherodt (Springer, Heidelberg, 1984), Vol. 54, p. 463.
[18] P. S. Peercy, G. A. Samara, and B. Morosin, J. Phys. Chem. Solids **35**, 1123 (1975).
[19] F. Cerdeira, F. E. A. Melo, and V. Lemos, Phys. Rev. B **27**, 7716 (1983).
[20] E. Liarokapis, E. Anastassakis, and G. A. Kourouklis, Phys. Rev. B **32**, 8346 (1985).
[21] Y. S. Raptis, G. A. Kourouklis, E. Anastassakis, E. Haro, and M. Balkanski, J. Phys. (Paris) **48**, 239 (1987).
[22] J. Cai, C. Raptis, Y. S. Raptis, and E. Anastassakis, Phys. Rev. B **51**, 201 (1995).
[23] A. Perakis, E. Sarantopoulou, Y. S. Raptis, and C. Raptis, Phys. Rev. B **59**, 775 (1999).
[24] P. Blanchfield, Tu Hailing, A. J. Miller, G. A. Saunders, and B. Chapman, J. Phys. C **20**, 3851 (1983).
[25] L. Misiak, P. Mikolajczak, and M. Subotowicz, Phys. Status Solidi A **97**, 353 (1986).
[26] M. Gluyas, F. D. Hughes, and B. W. James, J. Phys. D **6**, 2025 (1973).
[27] P. Blanchfield and G. A. Saunders, J. Phys. C **12**, 4673 (1979).
[28] E. Sarantopoulou, C. Raptis, G. A. Kourouklis, and S. Ves (unpublished).
[29] X. X. Zhang, A. B. Villaverde, M. Bass, B. H. T. Chai, H. Weidner, R. I. Ramotar, and R. E. Pearle, J. Appl. Phys. **74**, 790 (1993).